A structural study and some magnetic properties of the (Sc,Nb)Fe2 series of compounds

S. El Bidaoui, L.V.B. Diop, F. Maccari, O. Isnard

A structural study and some magnetic properties of the (Sc,Nb)Fe_2 series of compounds

S. El Bidaoui[1], L. V. B. Diop[2], F. Maccari[3], O. Isnard[1]
[1]*Université Grenoble Alpes, Institut Néel, CNRS, BP166X, 38042 Grenoble Cédex 9, France*
[2]*Université de Lorraine, CNRS, IJL, F-54000 Nancy, France*
[3]*Institute of Materials Science, Technical University of Darmstadt, D-64287 Darmstadt, Germany*

Abstract:

We report on the effects of Nb for Sc substitution on the structural and magnetic properties of the $Sc_{1-x}Nb_xFe_2$ series of compounds by means of scanning electron microscopy, energy dispersive X-ray microanalysis, X-ray powder diffraction, and magnetic measurements. The study focus on hexagonal *P6₃/mmc* crystal symmetry structure of the $ScFe_2$ phase retained along the series. Whereas the unit cell is found to decrease regularly upon increasing the niobium content the magnetic properties are found to evolve in a non monotonous manner. A drop of the magnetization and Curie temperature is observed upon substitution, the highest T_C being 530 K. Indeed, it is shown that Nb for Sc substitution induces dramatic changes of the magnetic properties such as a strong decrease of the ordering temperature and significant reduction of the spontaneous magnetization for Nb content above x=0.2 and 0.1, respectively. The highest magnetization is found for the Sc rich side with values of about 2.6 μ_B/f.u. corresponding to 1.3 μ_B/Fe atom. Moreover, compounds with x=0.75 and 1 are no longer exhibiting ferromagnetic order even at 2 K. The easy magnetization direction of $Sc_{1-x}Nb_xFe_2$ series of compounds is determined to be along the *c*-axis at room temperature.

Keywords: transition metal intermetallics, X-ray diffraction, crystal structure, phase diagrams, magnetic measurements,

1. Introduction

Even though Laves phases are known for almost 90 years, they continue to attract much interest from the viewpoints of both technological applications and fundamental research. There is an unexpectedly wide range of prosperous utilization of Laves phases in functional applications including Laves type intermetallic compounds as hydrogen storage materials, for wear- and corrosion-resistant coatings in corrosive atmospheres and at high temperatures, or as magneto-mechanical sensors and actuators, to name but a few [1]. Furthermore, large magnetocaloric effect and giant negative thermal expansion (NTE) have recently been discovered in some Laves phases compounds [2,3]. The magnetocaloric effect can be used for solid-state magnetic refrigeration, a very promising technological alternative to conventional gas-compression/expansion cooling. Solids exhibiting NTE properties have huge industrial merit as they can be utilized to control and tailor the overall thermal expansion of materials in many fields like aerospace and high-precision optics.

Fe-based Laves phases AFe$_2$, where A can be a 3*d*, 4*d*, 5*d*, or rare-earth element, have been a subject of extensive theoretical and experimental studies owing to the strong correlations between magnetism and crystal lattice in these compounds. Various types of crystal structure and magnetic ordering appear depending upon the species at the A site. Laves family of compounds consists of three parent members: the C36 hexagonal MgNi$_2$-type (*P6$_3$/mmc*), the C15 cubic MgCu$_2$-type (*Fd-3m*), and the C14 hexagonal MgZn$_2$-type (*P6$_3$/mmc*) structures. For example, HfFe$_2$ and ScFe$_2$ are ferromagnets [4,5] whereas TiFe$_2$ presents an antiferromagnetic ground state [6]. NbFe$_2$ is a rare itinerant intermetallic system displaying a chemically mediated magnetic quantum criticality [7,8]. By varying the nonthermal control parameter such as chemical doping in the Nb$_{1-y}$Fe$_{2+y}$ composition series, three distinct ground state phases near a quantum critical point (QCP) can be accessed across a small composition region at ambient pressure [9,10]. At slightly off-stoichiometric concentrations, both towards the Nb-rich and the Fe-rich side, Nb$_{1-y}$Fe$_{2+y}$ intermetallics are weakly ferromagnetic at low temperature. At or very close to stoichiometry, an antiferromagnetic, or spin-density-wave (SDW) order emerges on top of the ferromagnetic phase. Moreover, in between Nb-rich and stoichiometric composition, a quantum critical point/regime is observed where the SDW state collapses and non-Fermi-liquid behavior appears [7,11,8]. The Nb$_{1-y}$Fe$_{2+y}$ series of compounds exhibits a complex and intriguing phase diagram in which magnetism can easily be tuned by changes of the Nb/Fe stoichiometry, i.e., the magnetic ground state depends sensitively on the chemical composition. As NbFe$_2$ demonstrates a rich interplay of different types of magnetic ordering within a narrow

concentration range, this system constitutes an exceptional playground for condensed matter physics and tenders a good opportunity to examine ferromagnetic quantum criticality and the exact characteristics of critical phenomena of the QCP [12]. The discovery of QCP in $NbFe_2$ intermetallic compound opens up the new phenomenon of quantum tricriticality for experimental investigations in a whole class of materials with avoided or buried ferromagnetic QCP [13]. This offers fresh perspectives on other systems in which multiple and competing low-energy scales have in the past hidden the detection of a QCP and prevented the study of its consequences [10].

In the present work, we focus our study on AFe_2 compounds containing non-magnetic *A* element in order to gain a deeper insight into the magnetic behavior of the Fe-sublattice in the purposefully selected $(Sc,Nb)Fe_2$ pseudo-binary system. More recently an article has been published on the $Sc_{1-x}Nb_xFe_2$ series of compounds by Jin-Ting et *al.* [14]. $ScFe_2$ is polymorphic with both of the hexagonal C14 and C36 structures and also forms the cubic C15 $MgCu_2$-type structure [15,16]. In their recently published study, Jing-Ting and co-workers [14] reported on the crystal and some magnetic properties of $Sc_{1-x}Nb_xFe_2$ alloys composed of a mixture of hexagonal and cubic phases. However, this biphasic nature hampers to determine precisely the intrinsic properties of each crystal structure type. In order to complement this earlier study, we propose to focus our attention on the hexagonal $MgZn_2$ form of the $Sc_{1-x}Nb_xFe_2$ compounds. Additionally, the previously published magnetic results were restricted to temperature above 50 K and to a limited composition range. Here we aim to report on the low-temperature magnetic properties of the C14-type $Sc_{1-x}Nb_xFe_2$ series of compounds down to 2 K aiming to provide a more complete magnetic phase diagram.

2. Experimental techniques

Polycrystalline alloys with the $Sc_{1-x}Nb_xFe_2$ stoichiometry and x ranging from 0 to 1 were prepared by comelting appropriate amounts of the constituent metals on a water cooled copper hearth under a purified argon gas atmosphere in an arc melter. For better homogeneity, each sample (total weight ranging typically between 7 and 10 g) was arc-melted several times with the ingot being flipped over after each re-melting. The weight losses after melting were very low (<0.25 wt.%). The resulting buttons were placed in zirconia crucibles; these were put into quartz tubes and sealed off under a pressure of 0.2 bar of pure argon. The quartz ampoules were

placed into a resistive tube furnace for annealing at 1000 °C for seven days, and subsequently quenched in water.

The annealed samples were characterized by chemical analysis, by metallographic methods, as well as by standard x-ray diffractometry. The synthesized ingots were cut and polished for optical microscopy and scanning electron microscopy (SEM). The phase purity and the microstructure were analyzed with SEM in back scattered electron (BSE) contrast using a Tescan VEGA3 SBH microscope. The chemical composition of the observed phases was checked by energy- dispersive x-ray spectroscopy (EDS) microanalysis. Room temperature x-ray powder diffraction was carried out on a Stoe Stadi P diffractometer in transmission mode with Mo-$K_{\alpha 1}$ radiation (λ=0.70930 Å) over an angular 2θ range from 5° to 50° and a scan step of 0.01°. Rietveld refinements of the diffractograms were performed using the FullProf program [17].

In order to obtain optimal magnetic alignment, powder samples were sieved to a particle size smaller than 30 µm. Then the finely powdered particles were mixed with epoxy resin and subsequently aligned at room temperature by application of a magnetic field of typically 0.1 T until the epoxy resin has solidified. The field oriented powder particles were used for x-ray diffraction using copper $K_{\alpha 1,2}$ radiation λ = 1.5418 Å.

Magnetization measurements were undertaken on powder samples free to rotate in the sample holder, in static magnetic fields of up to 14 T at temperatures ranging from 2 to 400 K using a commercial vibrating-sample magnetometer (PPMS-14 of Quantum Design). Additional magnetization curves have been recorded on home-made extraction magnetometer [18]. The Curie temperature has been determined from the temperature dependence of the square of the magnetization recorded under 0.1 T.

3. Results and discussion

3.1. Crystal structure

$Sc_{1-x}Nb_xFe_2$ samples with nominal compositions ranging from x=0 up to x=1 have been prepared and characterized by systematic investigation using X-ray diffraction and electron scanning microscopy technique. The phase composition study performed by SEM reveals the presence of a complete solid solution. The $Sc_{1-x}Nb_xFe_2$ alloys exhibit a diffraction pattern featured by a single phase of *$P6_3/mmc$* symmetry of $MgZn_2$-type structure also referred to as C14. Traces of alpha iron have been found in some alloys with a content below 2% according to diffraction analysis, however the Rietveld refinement of the X-ray diffraction pattern reveals

that the retained crystal structure is purely hexagonal $MgZn_2$-type and no cubic phase is observed. The hexagonal C14 crystal structure is depicted in Fig. 1. Within the unit cell, the Fe atoms reside on two inequivalent crystal positions 2*a* (0, 0, 0) and 6*h* (*x*, 2*x*, 1/4) whereas the Sc/Nb atoms occupy one single Wyckoff site 4*f* (1/3, 2/3, *z*). The unit cell consists of 4 formula units and this atomic arrangement is representative of Frank-Kasper phase materials characterized by icosahedral polyhedron with low coordination of 12, labeled CN12. The Fe atoms at 2*a* position present an axial symmetry (-3m) and a local chemical environment which is composed of 12 near neighbors: 6 Sc/Nb atoms and 6 Fe located at 6*h*. Regardless of its different local symmetry, the Fe(6*h*) site possesses also 12 near neighbors: 6 of which are Sc/Nb ones, 2 Fe(2*a*) type and 4 Fe(6*h*) neighbors. The Sc/Nb atoms are surrounded by 16 neighbors: 9 Fe(6*h*) neighbors, 4 Sc/Nb atoms and 3 Fe(2*a*) neighbors. The crystal structure of $(Sc,Nb)Fe_2$ is featured by a double layer of Kagomé lattice sheets made by Fe atoms at 6*h* Wykoff position. The 6*h* Fe sites form two Kagomé networks which are perpendicular to the six-fold symmetry axis *c* and separated by Fe(2*h*) atoms in a hexagonal sub-lattice. The Sc/Nb atoms lie in Fe cages. In terms of crystallography, there are two distinct types of Fe atoms, which may exhibit different behavior from a magnetic point of view.

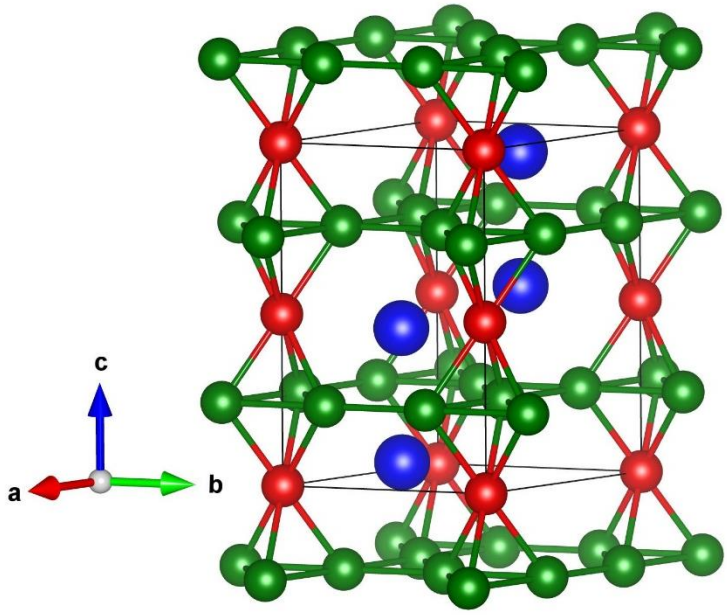

Fig.1. Hexagonal structure of $Sc_{1-x}Nb_xFe_2$ (space group $P6_3/mmc$). Sc or Nb(4*f*) in blue, Fe(2*a*) in red, and Fe(6*h*) in green.

x	a (Å)	c (Å)	V (Å^3)	M_S ($\mu_B/f.u.$)	T_C (K)
0	4.9741 (3)	8.1349 (6)	174.30 (2)	2.32 (5)	530 (5)
0.10	4.9637 (4)	8.1150 (9)	173.15 (3)	2.44 (5)	524 (5)
0.15	4.9590 (3)	8.1041 (5)	172.60 (2)	2.47 (5)	443 (5)
0.17	4.9540 (2)	8.0971 (3)	172.10 (1)	2.45 (5)	438 (5)
0.175	4.9519 (2)	8.0938 (5)	171.88 (2)	2.57 (5)	432 (5)
0.18	4.9521 (3)	8.0927 (5)	171.87 (2)	2.59 (5)	434 (5)
0.20	4.9492 (2)	8.0885 (4)	171.58 (2)	2.59 (5)	420 (5)
0.22	4.9460 (2)	8.0822 (3)	171.22 (1)	2.66 (5)	417 (5)
0.25	4.9390 (2)	8.0716 (5)	170.52 (2)	2.51 (5)	383 (5)
0.30	4.9298 (3)	8.0559 (5)	169.55 (2)	2.38 (5)	345 (5)
0.35	4.9232 (4)	8.0464 (7)	168.89 (2)	1.72 (5)	314 (5)
0.40	4.9158 (3)	8.0347 (5)	168.14 (2)	1.17 (5)	240 (5)
0.50	4.8974 (5)	8.0037 (8)	166.25 (3)	0.43 (5)	170 (5)
0.60	4.8851 (4)	7.9829 (6)	164.98 (2)	0.16 (5)	120 (5)
0.75	4.8664 (3)	7.9510 (6)	163.07 (2)	--	--
1	4.8426 (1)	7.8998 (3)	160.44 (1)	--	--

Table 1. Unit cell parameters as derived from x-ray diffraction experiments (refined by Le Bail method), spontaneous magnetization at 4 K, and transition temperature of the $Sc_{1-x}Nb_xFe_2$ compounds. The number in parenthesis are referring to the estimated error bars on the last decimal: three times the standard deviation.

The lattice parameters of the $Sc_{1-x}Nb_xFe_2$ series of alloys have been determined from least square refinement of the X-ray diffraction patterns. The corresponding values are summarized in Table 1 and plotted as a function of Nb concentration in Fig. 2. Nb for Sc substitution leads to a decrease of the unit cell volume as well as both *a* and *c* parameters. As can be seen from Fig. 2 the composition dependence of the lattice parameters follows an essentially linear behavior typical of Vegard's law. A mean reduction rate of $\Delta a/a$ = 2.7%, slightly larger along the *c*-axis $\Delta c/c$ = 2.98%, is observed upon substitution thus leading to an overall volume contraction of $\Delta V/V$ = 8.6%. For the intermediate composition range from approximately x=0.3 to 0.7 both cell parameters, *a* and *c*, are slightly smaller than the values expected from linearity. This observation is consistent with the results reported recently by Jin-Ting *et al.* [14].

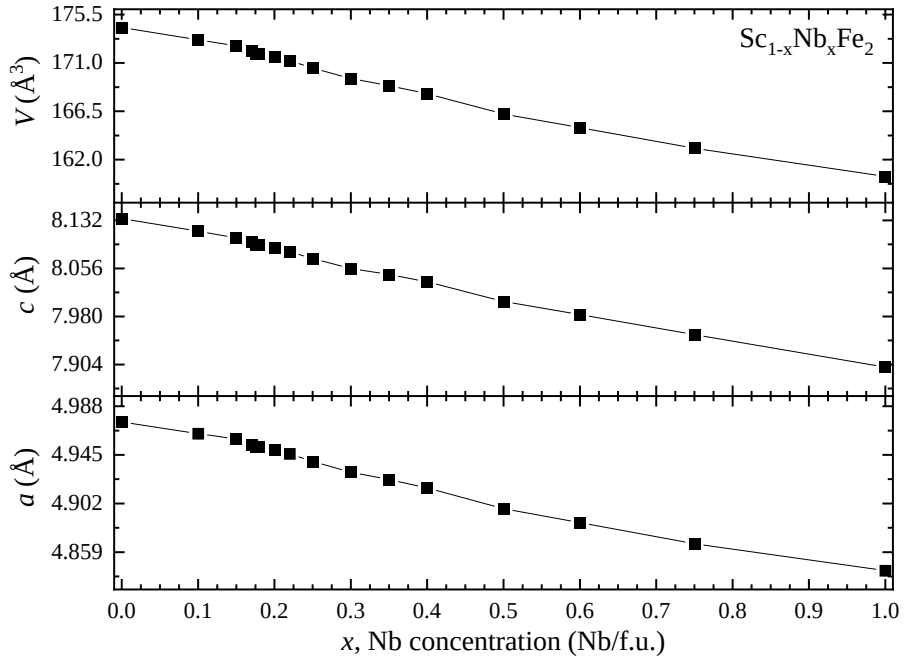

Fig. 2. Concentration dependences of unit cell parameters of the $Sc_{1-x}Nb_xFe_2$ compounds (refined by Le Bail method).

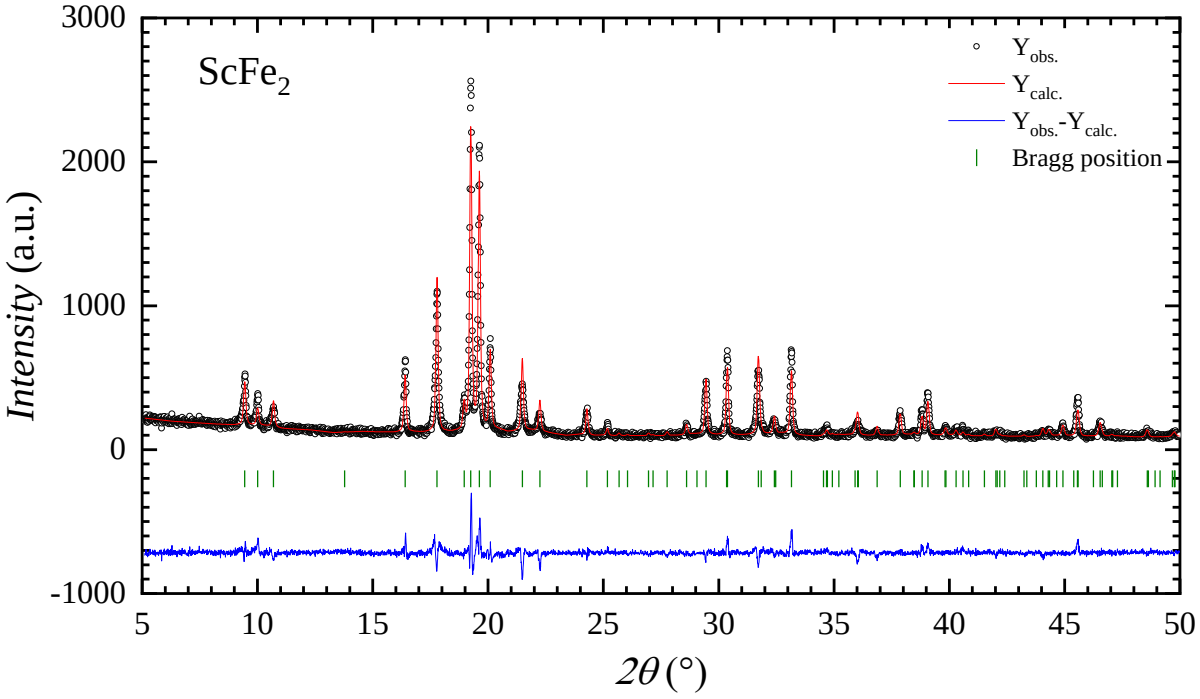

Fig. 3. X-ray powder diffraction pattern recorded at 300 K for $ScFe_2$ (source Mo, $K_{\alpha 1}$ radiation λ=0.70930 Å). The circles and red line refer to the data point and the fit to the data respectively. The tick below the diffraction pattern indicates the Bragg peak corresponding to the C14 hexagonal structure type. The blue line at the bottom represents the difference between the data and the calculated pattern.

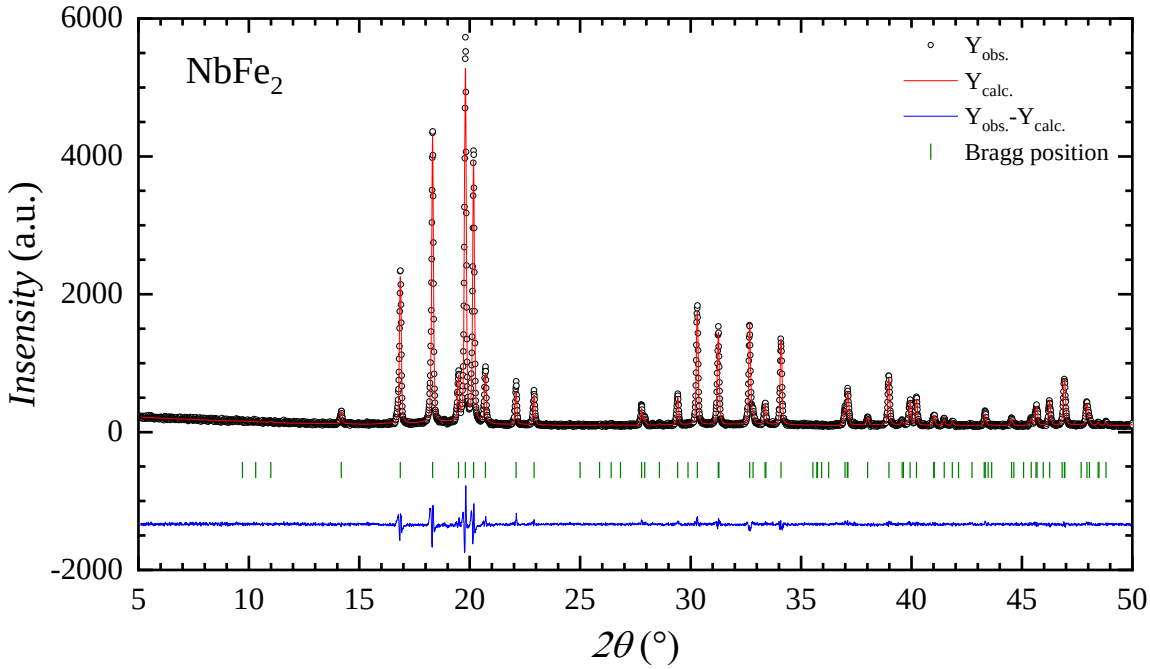

Fig. 4. X-ray powder diffraction pattern recorded at 300 K for $NbFe_2$ (source Mo, $K_{\alpha 1}$ radiation λ=0.70930 Å). The tick below the diffraction pattern indicates the Bragg peak corresponding to the C14 hexagonal structure type. The blue line at the bottom represents the difference between the data and the calculated pattern.

As shown by Rietveld analysis (see Figs. 3-4), the $Sc_{1-x}Nb_xFe_2$ compounds investigated here are retaining the same C14 structure type whatever the *x* value. It is then interesting to study the effect of Nb for Sc substitution on the local atomic environments. According to the Rietveld refinement results listed in Table 2, the Fe-Fe interatomic distances are much reduced upon Nb for Sc substitution. For instance, Fe(6*h*)-Fe(2*a*) distance decreases from 2.499 to 2.431 Å for $ScFe_2$ and $NbFe_2$, respectively. The reduction of Fe(6*h*)-Fe(6*h*) distance is of the same order of magnitude. This indicates that the Fe tetrahedral building blocks are essentially shrunk but not distorted along the Nb for Sc substitution. Another noteworthy point is that the Fe-Fe interatomic distances are close to or below 2.5Å for $ScFe_2$ and strongly reduced upon increasing x, down to 2.45 or 2.43Å below the sum of metallic radii (1.27Å [19]). Such shrinkage is expected to reduce the strength of the exchange interactions and even lead locally to negative Fe-Fe exchange interactions according to the Néel-Bethe-Slater curve [20]. This clearly contributes to the observed drop of the Curie temperature upon Nb for Sc substitution. Theoretical calculations performed on $MgCo_2$ [21] and $(Hf,Ta)Fe_2$ [22] Laves phases with the hexagonal structure have demonstrated that the ferromagnetic order in these compounds is controlled by the Co-Co and Fe-Fe interatomic distances, respectively. For the pseudo-binary system $(Hf,Ta)Fe_2$, a detailed investigation of the interatomic Fe-Fe exchange coupling

coefficients and their lattice dependence revealed that the ferromagnetic interaction with the first shell is strongly reduced upon shrinkage of the *a* lattice constant [22]. Another noteworthy observation in the first principles electronic structure calculations reported in Ref. [22] is that the Fe(*6h*)-Fe(*6h*) coupling is always positive indicating that these interactions will favour a ferromagnetic spin arrangement within the atomic plane containing the Fe(*6h*) crystal sites with Fe(*6h*) as near neighbours. The magnetic phase transition was found to be accompanied by a sharp diminution of the Fe(*2a*)-Fe(*6h*) exchange parameters for the first neighbours [22]. Similar mechanism may be involved here for the observed reduction of T_C.

	$ScFe_2$	$Sc_{0.85}Nb_{0.15}Fe_2$	$NbFe_2$
a (Å)	4.974 (3)	4.953 (2)	4.840 (2)
c (Å)	8.135 (5)	8.096 (3)	7.896 (2)
$z_{Sc(4f)}$	0.0547 (4)	0.0611 (2)	0.0632 (2)
$x_{Fe(6h)}$	0.8315 (5)	0.8311 (4)	0.8308 (4)
$y_{Fe(6h)} = 2x_{Fe(6h)}$	1.663 (1)	1.662 (1)	1.662 (1)
$\beta_{Sc/Nb}$ (Å^2)	0.187 (63)	0.826 (45)	0.366 (23)
β_{Fe} (Å^2)	1.212 (53)	1.092 (36)	0.390 (27)
χ^2	2.11	1.49	1.81
R_{Bragg} (%)	11.3	5.12	3.21
R_{wp} (%)	11.4	10.4	9.09
R_p (%)	8.89	8.07	7.12
R_{exp} (%)	8.02	8.85	7

Table 2. Unit cell parameters, atomic coordinates, displacement parameters, and confidence factors from Rietveld refinement of the XRD pattern at 300 K for $ScFe_2$, $Sc_{0.85}Nb_{0.15}Fe_2$, and $NbFe_2$

Atom	Number of neighbors	Neighbor	Distances (Å) $ScFe_2$	Distances (Å) $Sc_{0.85}Nb_{0.15}Fe_2$	Distances (Å) $NbFe_2$
Sc/Nb (4*f*)	3	Sc/Nb (4*f*)	3.0065(14)	3.0259(11)	2.9673(5)
	1	Sc/Nb (4*f*)	3.178(5)	3.059(3)	2.9503(16)
	3	Fe (2*a*)	2.9060(5)	2.9021(4)	2.83874(19)
	6	Fe (6*h*)	2.951(3)	2.9107(17)	2.8344(19)

	3	Fe (6*h*)	2.857(3)	2.887(2)	2.8299(15)
Fe (2*a*)	6	Fe (6*h*)	2.4987(15)	2.4892(14)	2.4308(14)
	6	Sc/Nb (4*f*)	2.9060(5)	2.9021(4)	2.83874(19)
Fe (6*h*)	2	Fe (6*h*)	2.460(3)	2.443(3)	2.3834(19)
	2	Fe (6*h*)	2.514(3)	2.510(3)	2.4569(19)
	2	Fe (2*a*)	2.4987(15)	2.489(1)	2.4308(10)
	2	Sc/Nb (4*f*)	2.857(3)	2.887(2)	2.8299(13)
	4	Sc/Nb (4*f*)	2.951(3)	2.911(2)	2.8344(19)

Table 3. Interatomic distances for $ScFe_2$, $Sc_{0.85}Nb_{0.15}Fe_2$ and $NbFe_2$

3.2. Magnetic properties

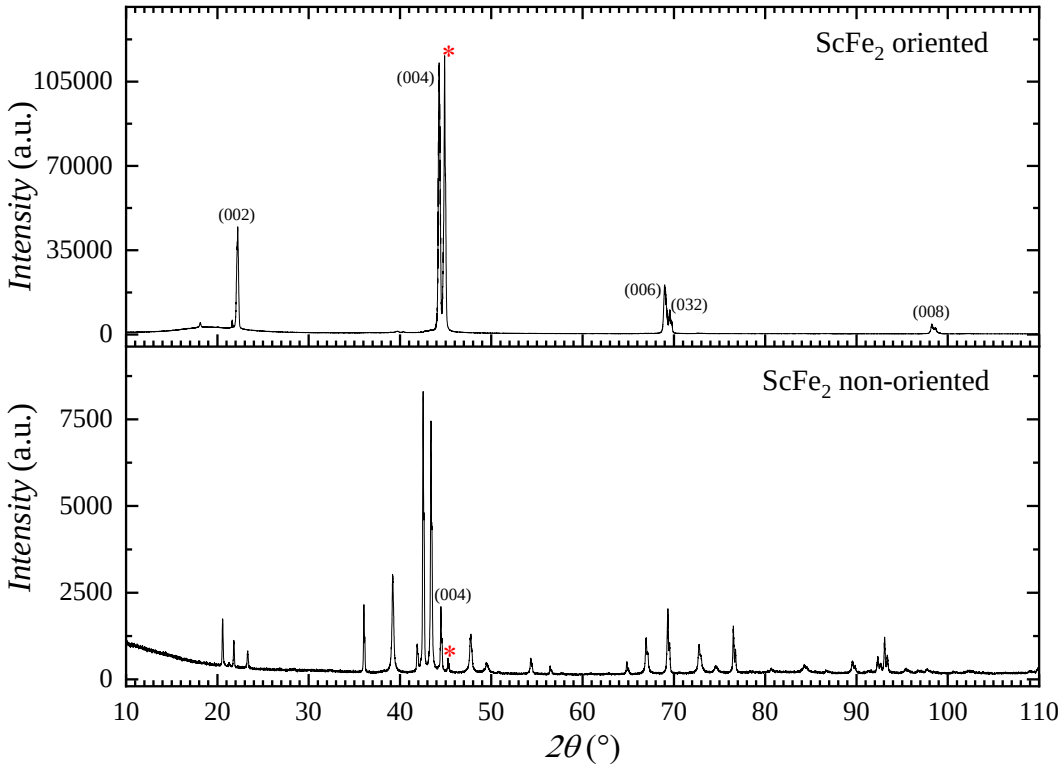

Fig. 5. X-ray diffraction patterns recorded (source Cu, $K_{\alpha 1,2}$ radiation λ = 1.5418 Å) on non-oriented and on magnetic field oriented $ScFe_2$. The star * refers to the (110) Bragg peak position of α-iron. All other Bragg peaks are indexed in *$P6_3/mmc$* space group.

Figure 5 presents a comparison of the X-ray diffraction pattern recorded on powder sample of $ScFe_2$ with the pattern recorded on the powder oriented under applied magnetic field. It is clearly seen that most Bragg peaks have disappeared upon application of magnetic field

except the (00*l*) ones whose intensity is enhanced. This is a proof that the easy magnetization direction of the $ScFe_2$ compound is along the *c* crystal axis. This finding is in good agreement with Mössbauer spectroscopy data reported in Ref. [23]. It is worth to point out that we have performed similar field orientation of $Sc_{1-x}Nb_xFe_2$ powder samples for x= 0.3 and 0.15. The corresponding X-ray diffraction patterns are also featured by highly enhanced (00*l*) Bragg peaks indicating that the *c* crystal axis is also the easy magnetization direction for such compounds.

The magnetic ordering temperature have been determined from the temperature dependence of the magnetization. The thermomagnetic curves are plotted in Figure 6 between 200 K and 800 K for the $Sc_{1-x}Nb_xFe_2$ compounds with composition ranging from x=0 to 0.25. In addition to the ferromagnetic behaviour exhibited by the temperature dependence of magnetization, one can remark the progressive reduction of the Curie temperature T_C upon increasing Nb content. The Curie temperature values are summarized in Table 1 whereas the composition dependence is illustrated in Figure 8. It is worth noting that a Curie temperature of 530(5) K is observed here for $ScFe_2$ in the C14 structure type, a value much lower than that reported previously in Ref. [14] for a biphasic mixture with the cubic form. This is probably due to a higher ordering temperature for the cubic form. The Curie temperature of the $Sc_{1-x}Nb_xFe_2$ samples is about the same up to x=0.1 then a progressive decrease is observed upon increasing the Nb content. As neither Sc nor Nb are expected to be magnetic, we can ascribe this decrease to the Fe sublattice only. A quasi-linear behaviour is found with a rate of 200 K/Nb atom in the range from x =0.1 to 0.6.

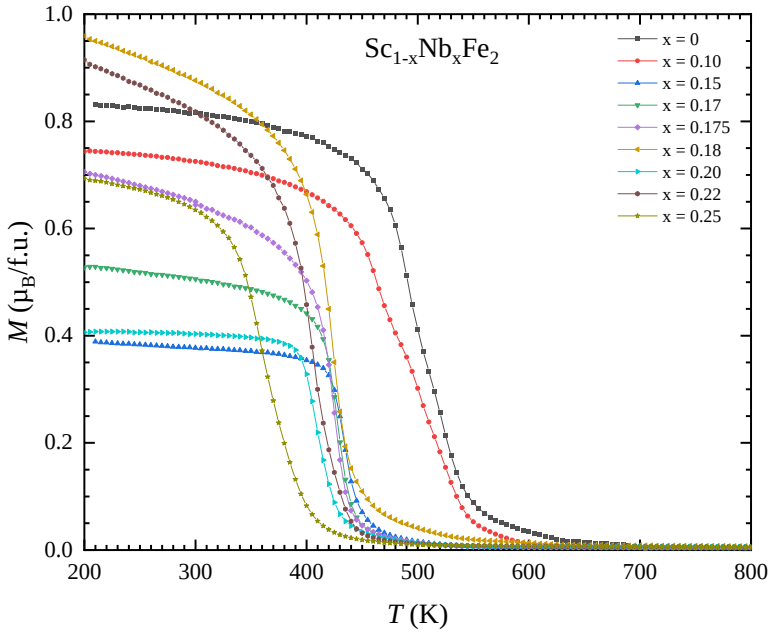

Fig. 6. Temperature dependence of magnetization for $Sc_{1-x}Nb_xFe_2$ under H= 0.1 T.

In order to determine the intrinsic magnetization of the $Sc_{1-x}Nb_xFe_2$ compounds in the ground state, magnetization isotherms were recorded at 5 K. The corresponding curves are plotted in Figure 7. The spontaneous magnetization, M_S, is deduced from such isothermal magnetization curves, and the corresponding values are listed in Table 1. The most striking feature is the large drop of the spontaneous magnetization above x=0.35 whereas high values of spontaneous magnetization are observed in the concentration range from x=0 to about 0.30. The composition dependence of the spontaneous magnetization is reported in Figure 8. The Sc rich side of the solid solution exhibits the highest magnetization values with a value approaching 2.5 μ_B/f.u., however, a strong decrease of M_S is observed for x> 0.3 and vanishes for composition above x= 0.6. This indicates a large effect of the Nb for Sc substitution on the *3d* electron magnetism of the Fe sublattice atoms.

The different behaviour of the composition dependence of M_S and T_C clearly indicates that the trend of T_C is not only driven by M_S evolution. In particular the non-monotonous trend of M_S(x) most probably reflects the importance of the electronic structure on the Fe sites. In other words, T_C is not uniquely dependent upon M_S change, but reflect the evolution of the lattice change, that induces modification of the Fe-Fe exchange interactions. Electronic band structure calculations could be interesting to investigate the origin of this composition dependence of the Curie temperature and M_S along the (Sc,Nb)Fe_2 series of compounds.

For the Sc rich side of the $Sc_{1-x}Nb_xFe_2$ compounds, the spontaneous magnetization values lead to a mean Fe magnetic moment of about 1 to 1.25 μ_B/ Fe atom; a value in agreement with earlier reported results on $ScFe_2$ [24]. Such atomic magnetic moment is about twice smaller than the 2.2 μ_B moment in elemental Fe. The maximum magnetization value is obtained for x=0.22 with 2.6 μ_B/f.u. but the magnetization value strongly decreases above x=0.3 and vanishes for 0.75 and x=1. The absence of spontaneous magnetization for $NbFe_2$ compound is in good agreement with earlier investigations and confirms that the compound is not over-stoichiometric in Fe. We will not further investigate the case of $NbFe_2$ which has been extensively studied elsewhere [13,25,26].

In order to illustrate the temperature dependence of the isothermal magnetization, several magnetization curves are represented in Figure 9 for $Sc_{0.8}Nb_{0.2}Fe_2$ in the temperature range from 4 to 500 K. The observed behaviour confirms that the ordering temperature is between 400 and 450 K in good agreement with the 420 K reported in Table 1, as derived from the thermomagnetic curves.

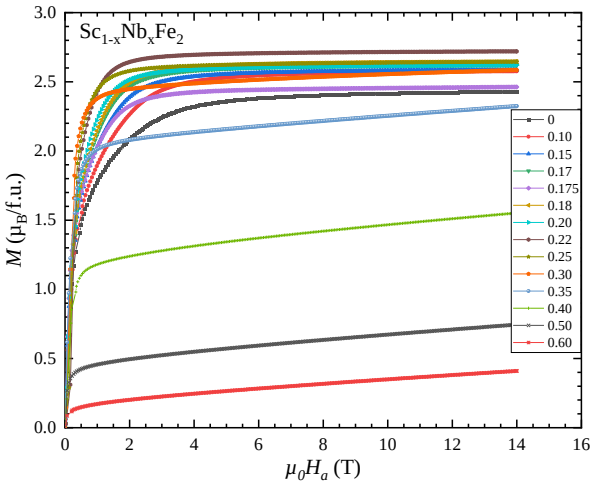

Fig. 7. Isothermal magnetization curves recorded for $Sc_{1-x}Nb_xFe_2$ at 5 K (PPMS-VSM)

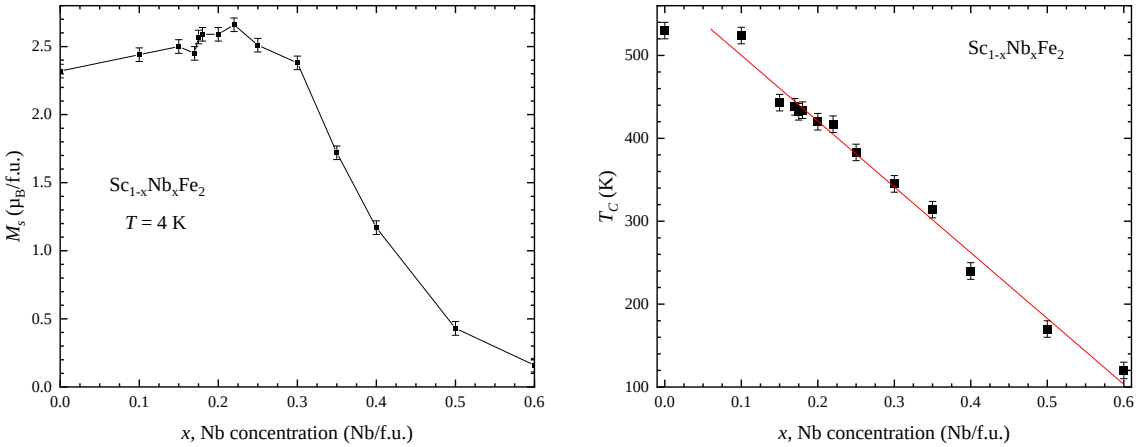

Fig. 8. Concentration dependences of spontaneous magnetization (left) and transition temperature (right) for $Sc_{1-x}Nb_xFe_2$ compounds.

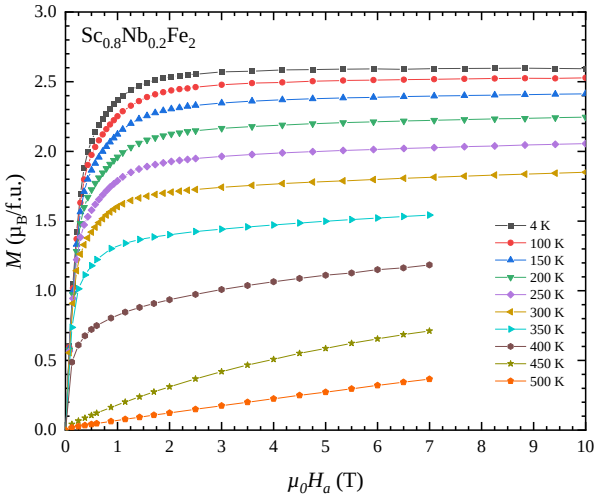

Fig. 9. Isothermal magnetization curves for $Sc_{0.8}Nb_{0.2}Fe_2$ at various indicated temperatures from 4 to 500 K.

4. Conclusion

A series of $Sc_{1-x}Nb_xFe_2$ alloy samples have been synthesized and their crystal structure and chemical composition investigated combining different experimental techniques. A complete solid solution of Nb has been observed for $Sc_{1-x}Nb_xFe_2$ compounds. All the lattice parameters are decreased upon Nb for Sc substitution in an essentially isotropic manner; the reduction being about 2.7 to 2.9% for *a* and *c*, respectively. We also reported the evolution of the ordering temperature versus Nb content along the $Sc_{1-x}Nb_xFe_2$ series of compounds and extending the magnetic phase diagram previously reported up to x=0.35 only. It is demonstrated that Nb for Sc substitution leads to a strong decrease of both the ordering temperature and the spontaneous magnetization.

References:

[1] F. Stein, A. Leineweber, Laves phases: a review of their functional and structural applications and an improved fundamental understanding of stability and properties, J Mater Sci 56 (2021) 5321–5427. https://doi.org/10.1007/s10853-020-05509-2.

[2] V. Paul-Boncour, T. Mazet, Investigation of compounds for magnetocaloric applications: $YFe_2H_{4.2}$, $YFe_2D_{4.2}$, and $Y_{0.5}Tb_{0.5}Fe_2D_{4.2}$, Journal of Applied Physics 105 (2009) 013914. https://doi.org/10.1063/1.3055348.

[3] B. Li, X.H. Luo, H. Wang, W.J. Ren, S. Yano, C.-W. Wang, J.S. Gardner, K.-D. Liss, P. Miao, S.-H. Lee, T. Kamiyama, R.Q. Wu, Y. Kawakita, Z.D. Zhang, Colossal negative thermal expansion induced by magnetic phase competition on frustrated lattices in Laves phase compound (Hf,Ta)Fe_2, Phys. Rev. B 93 (2016) 224405. https://doi.org/10.1103/PhysRevB.93.224405.

[4] K. Ikeda, T. Nakamichi, T. Yamada, M. Yamamoto, Ferromagnetism in Fe_2Sc with the Hexagonal $MgZn_2$-Type Structure, J. Phys. Soc. Jpn. 36 (1974) 611–611. https://doi.org/10.1143/JPSJ.36.611.

[5] T. Nakamichi, K. Kai, Y. Aoki, K. Iekda, M. Yamamoto, Ferromagnetism in the Laves Phase Compound $Fe_{2+x}Hf_{1-x}$ Annealed at 1000°C, J. Phys. Soc. Jpn. 29 (1970) 794–794. https://doi.org/10.1143/JPSJ.29.794.

[6] T. Nakamichi, Ferro- and Antiferromagnetism of the Laves Phase Compound in Fe-Ti Alloy System, J. Phys. Soc. Jpn. 25 (1968) 1189–1189. https://doi.org/10.1143/JPSJ.25.1189.

[7] A. Alam, D.D. Johnson, Chemically Mediated Quantum Criticality in $NbFe_2$, Phys. Rev. Lett. 107 (2011) 206401. https://doi.org/10.1103/PhysRevLett.107.206401.

[8] M. Brando, W.J. Duncan, D. Moroni-Klementowicz, C. Albrecht, D. Grüner, R. Ballou, F.M. Grosche, Logarithmic Fermi-Liquid Breakdown in $NbFe_2$, Phys. Rev. Lett. 101 (2008) 026401. https://doi.org/10.1103/PhysRevLett.101.026401.

[9] T.D. Haynes, I. Maskery, M.W. Butchers, J.A. Duffy, J.W. Taylor, S.R. Giblin, C. Utfeld, J. Laverock, S.B. Dugdale, Y. Sakurai, M. Itou, C. Pfleiderer, M. Hirschberger, A. Neubauer, W. Duncan, F.M. Grosche, Ferrimagnetism in Fe-rich $NbFe_2$, Phys. Rev. B 85 (2012) 115137. https://doi.org/10.1103/PhysRevB.85.115137.

[10] S. Friedemann, M. Brando, W.J. Duncan, A. Neubauer, C. Pfleiderer, F.M. Grosche, Ordinary and intrinsic anomalous Hall effects in $Nb_{1-y}Fe_{2+y}$, Phys. Rev. B 87 (2013) 024410. https://doi.org/10.1103/PhysRevB.87.024410.

[11] D. Moroni-Klementowicz, M. Brando, C. Albrecht, W.J. Duncan, F.M. Grosche, D. Grüner, G. Kreiner, Magnetism in $Nb_{1-y}Fe_{2+y}$: Composition and magnetic field dependence, Phys. Rev. B 79 (2009) 224410. https://doi.org/10.1103/PhysRevB.79.224410.
[12] A. Subedi, D.J. Singh, Band structure and itinerant magnetism in quantum critical $NbFe_2$, Phys. Rev. B 81 (2010) 024422. https://doi.org/10.1103/PhysRevB.81.024422.
[13] S. Friedemann, W.J. Duncan, M. Hirschberger, T.W. Bauer, R. Küchler, A. Neubauer, M. Brando, C. Pfleiderer, F.M. Grosche, Quantum tricritical points in $NbFe_2$, Nature Phys 14 (2018) 62–67. https://doi.org/10.1038/nphys4242.
[14] Z. Jing-Ting, H. Yibole, B. Narsu, Z.Q. Ou, O. Haschuluu, O. Tegus, F. Guillou, Structural and magnetic properties of $Sc_{1-x}Nb_xFe_2$ intermetallics showing anomalous zero thermal expansion, Intermetallics 136 (2021) 107252. https://doi.org/10.1016/j.intermet.2021.107252.
[15] K.A. Gschneidner, Jr., V.K. Pecharsky, Binary rare earth Laves phases — an overview, Zeitschrift Für Kristallographie - Crystalline Materials 221 (2006) 375–381. https://doi.org/10.1524/zkri.2006.221.5-7.375.
[16] V. Pokatilov, V. Golikova, A. Tsvyashchenko, L. Fomichova, Hyperfine fields and magnetic moments in intermetallic $ScFe_2$ with cubic and hexagonal structures, Hyperfine Interact 59 (1990) 529–532. https://doi.org/10.1007/BF02401289.
[17] J. Rodríguez-Carvajal, Recent advances in magnetic structure determination by neutron powder diffraction, Physica B: Condensed Matter 192 (1993) 55–69. https://doi.org/10.1016/0921-4526(93)90108-I.
[18] A. Barlet, J.C. Genna, P. Lethuillier, Insert for regulating temperatures between 2 and 1000 K in a liquid helium dewar: description and cryogenic analysis, Cryogenics 31 (1991) 801–805.
[19] E.T. Teatum, Jr. Gschneidner K.A., J.T. Waber, Compilation of calculated data useful in predicting metallurgical behavior of the elements in binary alloy systems., 1968. https://doi.org/10.2172/4789465.
[20] L. Néel, Propriétés magnétiques de l'état métallique et énergie d'interaction entre atomes magnétiques, Ann. Phys. 11 (1936) 232–279. https://doi.org/10.1051/anphys/193611050232.
[21] V.A. Yartys, P. Vajeeston, R.V. Denys, L. Havela, S. Maskova-Cerna, A. Szytula, Bonding mechanism and magnetic ordering in Laves phase λ_1–$MgCo_2$ intermetallic compound from theoretical and experimental studies, Scripta Materialia 237 (2023) 115709. https://doi.org/10.1016/j.scriptamat.2023.115709.
[22] L.V.B. Diop, D. Benea, S. Mankovsky, O. Isnard, Cross over between ferro and antiferromagnetic order in Fe itinerant electron magnetism: An experimental and theoretical study of the model (Hf,Ta)Fe_2 Laves phases, Journal of Alloys and Compounds 643 (2015) 239–246. https://doi.org/10.1016/j.jallcom.2015.04.134.
[23] P.H. Smit, K.H.J. Buschow, Fe 57 Mössbauer effect in $ScFe_2$ and $ScFe_2H_2$, Phys. Rev. B 21 (1980) 3839–3843. https://doi.org/10.1103/PhysRevB.21.3839.
[24] S.G. Sankar, W.E. Wallace, Magnetic properties of $ScFe_2$, AIP Conference Proceedings 29 (1976) 334–334. https://doi.org/10.1063/1.30654.
[25] D. Margineda, J.A. Duffy, J.W. Taylor, S.R. Giblin, μSR study of stoichiometric $NbFe_2$, Physica B: Condensed Matter 504 (2017) 121–126. https://doi.org/10.1016/j.physb.2016.10.014.
[26] M. Bałanda, S.M. Dubiel, On the magnetism of the C14 $Nb_{0.975}Fe_{2.025}$ Laves phase compound: Determination of the H-T phase diagram, Journal of Magnetism and Magnetic Materials 454 (2018) 386–391. https://doi.org/10.1016/j.jmmm.2018.01.055.